PULBERI DE SnO_2 DOPATE CU La^{3+} SAU V^{5+}

SnO_2 POWDERS DOPED WITH La^{3+} OR V^{5+}

ANDREI-DAN BUSUIOC, RAMONA ENUŢĂ, ŞTEFANIA STOLERIU *, OVIDIU OPREA, TEODOR VIŞAN
University POLITEHNICA of Bucharest, RO-011061, Bucharest, Romania

La^{3+} or V^{5+} doped SnO_2 powders were synthesized by the precipitation method, the crystalline phases being obtained after a thermal treatment at 400 °C. The calcined samples were characterized in terms of crystalline structure, morphology and optical properties by employing X-ray diffraction, scanning electron microscopy and UV-Vis spectroscopy. The results indicate that both doping cations modify the average crystallite size and bandgap of SnO_2 based materials, while their concentration permits a fine tuning of the functional features.

Pulberile de SnO_2 dopate cu La^{3+} sau V^{5+} au fost sintetizate prin metoda precipitării, fazele cristaline fiind obţinute după un tratament termic la 400 °C. Probele calcinate au fost caracterizate în ceea ce priveşte structura cristalină, morfologia şi proprietăţile optice prin utilizarea difracţiei de raze X, a microscopiei electronice cu baleiaj şi a spectroscopiei în UV-Viz. Rezultatele indică faptul că ambii cationi dopanţi modifică dimensiunea medie a cristalitelor şi banda interzisă a materialelor pe bază de SnO_2, în timp ce concentraţia acestora permite ajustarea fină a proprietăţilor funcţionale.

Keywords: *Semiconductor Oxides; Precipitation Method; Dopants; Bandgap; Gas Sensors*

1. Introduction

The field of gas sensors is of great importance both for a wide range of industries that involve working with gaseous species, but also for the environmental monitoring and human safety reasons, for which sever requirements have been adopted lately. Thus, a chemical gas sensor is a device which mimics the olfactory discrimination mechanism [1] and signals/prevents the possible occurrence of disastrous events. Those materials that change their properties in the presence of a specific gas in the local environment are suitable for the development of gas detection devices, these monitoring in real time the concentration of particular gases and providing a quantifiable and precise response, in correlation with the variation of the electrical conductivity [2].

In this context, tin dioxide (SnO_2), a *n* type semiconductor, with a large bandgap of about 3.6 eV, is one of the most used material from its category [3, 4] due to the well known chemical stability and mechanical properties. SnO_2 conductivity mainly originates from the oxygen vacancies, which means that the corresponding structures are non-stoechiometric [5], with a concentration of defects that is hard to control. Moreover, SnO_2 is an oxide material that combines the electric resistance with a high optical transparency. In particular, SnO_2 based gas sensors are characterized by low production cost, high sensitivity and fast response, features that represent a guarantee for the implementation of safety measures at different scales.

SnO_2 is rarely used in its pure form, generally being loaded with impurities or dopants. In gas detection, these additives increase the sensitivity and selectivity for certain gases [6]. The employed dopants are heterovalents, with lesser or grater valence, fact that leads to a material with *n* or *p* conduction. Moreover, this oxide has been obtained in different morphological forms, from bulk [7] to thin films [8, 9], from one dimensional structures [10, 11] to zero dimensional ones [12-14], aspect that confirms the extended interest of the scientific community for the integration of SnO_2 in miniaturized and more efficient devices. Going to the synthesis, the wet chemistry methods present several advantages over the conventional ones, providing a good control of stoechiometry, purity, homogeneity and morphology, while significantly reducing the processing temperature [15-17]. From this category, precipitation [18, 19], sol-gel [20], hydrothermal [21], combustion [12] and pyrolysis [22] methods can be mentioned. Thus, the remarkable electrical and optical properties possessed by SnO_2 recommend it for a wide range of applications: gas sensors [9, 11, 13], transparent electrodes for solar cells [23], anodes for ion batteries [14], photocatalysts [12], biosensors [24], as well as magnetic devices [18].

* Autor corespondent/*Corresponding author*,
E-mail: stefania.stoleriu@upb.ro

In this work, we report on the synthesis and characterization of La^{3+} or V^{5+} doped SnO_2 powders. The dopants selection was based on the existence of a small number of scientific papers dedicated to this specific direction. They were added in order to modify the morphology and optical features of the corresponding materials, so that to achieve tuned properties, suitable for the development of gas sensing devices. The phase composition, crystalline structure, microstructural and semiconductor properties were investigated and correlations were established.

2.Experimental

SnO_2 powders were prepared by the precipitation method, using tin chloride dihydrate ($SnCl_2 \cdot 2H_2O$, ≥ 98 %, Sigma-Aldrich), lanthanum oxide (La_2O_3, ≥ 99.99 %, Fluka) and ammonium metavanadate (NH_4VO_3, ≥ 99.99 %, Sigma-Aldrich) as starting materials. $SnCl_2 \cdot 2H_2O$ was weighted according to the desired quantity of final material and dissolved in a minimum volume of distilled water. To this clear solution, the dopant solution obtained by solubilising La_2O_3 or NH_4VO_3 in 37 % hydrochloric acid was added, so that to provide 0.5, 1.0 or 2.0 wt.% concentration of dopant. After an intense homogenisation at room temperature for 1 h, the *p*H was switched to basic values (*p*H = 11 - 12) with the help of a 25 % ammonia solution, which led to the precipitation of Sn^{2+} ions in the form of $Sn(OH)_n$, where n = 2 or 4, or/and other hydrated tin species [25]. The resulting suspension was filtered and the white precipitate was collected, being subsequently washed for several times with distilled water until neutral *p*H. Further, the precipitate was dried at 80 °C for 24 h, followed by calcination at 400 °C for 2 h in order to achieve a crystalline oxide phase.

The as-obtained precipitate was subjected to thermal analysis in air, in the 20 - 1000 °C temperature range, this being performed on a Shimadzu DTG-60 equipment. The calcined powders were investigated by X-ray diffraction (XRD), scanning electron microscopy (SEM) and UV-Vis spectroscopy. A Shimadzu XRD 6000 diffractometer with Ni filtered Cu Kα radiation (λ = 0.154 nm) was employed to identify the phase composition and crystalline structure of the samples, 2θ ranging between 20 and 80 °. The average crystallite size (D) was calculated using Scherrer equation: $D=K \cdot \lambda/(\beta \cdot \cos\theta)$, where K is a dimensionless shape factor with a typical value of about 0.9, λ is the X-ray wavelength (0.154 nm), β is the full width at half maximum (FWHM) value corresponding to (110) diffraction peak and θ is Bragg angle. A Quanta Inspect F scanning electron microscope was used to visualize the powders morphology. The reflectance spectra were recorded with a Jasco V 560 UV-Vis spectrophotometer. In order to estimate the bandgap values, Kubelka-Munk functions ($F(R)$) were calculated using the reflectance data and $[F(R) \cdot E]^2$ functions were plotted versus photon energy (E); Kubelka-Munk function is expressed as $F(R)=(1-R)^2/(2 \cdot R)$, where R is the observed diffuse reflectance.

3.Results and discussion

The thermal analyses performed on the dried precipitate is presented in Figure 1.

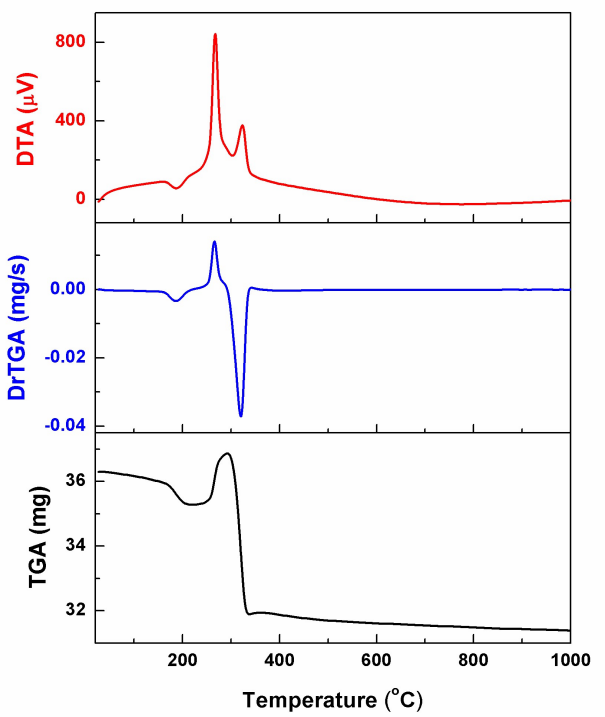

Fig. 1 - Thermal analysis performed on the dried precipitate: TGA - thermogravimetric analysis, DrTGA - the derivative of the themogravimetric analysis with respect to time and DTA - differential thermal analysis / *. Analiza termică realizată pe precipitatul uscat: TGA - analiză termogravimetrică, DrTGA - derivata analizei termogravimetrice în raport cu timpul şi DTA - analiză termică diferenţială.*

The DTA curve reveals three thermal effects, the first one endothermic and centred at approximately 185 °C, while the second and the third ones exothermic, with maxima at about 265 and 325 °C. By correlating the calorimetric information with the gravimetric data, the following explanations can be proposed. The first effect can be related to the decomposition/dehydration of the less stable tin hydrated species, with a weight loss around 3 %; the result consists in the formation of a small quantity of SnO phase. The second effect, which is also the strongest, can be associated with the oxidation of Sn^{2+} to Sn^{4+} since it is accompanied by a weight gain of about 4.5 %. When it comes to the third effect, the behaviour of the material is not very clear and only assumptions can be formulated. Thus, we suppose that the more stable tin hydrated species suffer a process

of decomposition/dehydration (endothermic effect), over which it overlaps an oxidation reaction (exothermic effect), the overall effect being exothermic; the plotted results indicate that the oxidation is much more intense that the other process, leading to the obtaining of SnO_2 phase [25]. Above 340 °C no significant weight loss is noticed, fact that validate a calcination temperature of 400 °C, when the samples are converted into crystalline oxide powders.

Figure 2 shows the XRD patterns of the calcined powders synthesized by the precipitation method. All diffraction peaks were assigned to SnO_2 compound with tetragonal structure (JCPDS 01-080-6727), fact demonstrated by the indexed maxima. Only for the high concentrations of dopant, some supplementary peaks seem to emerge, which can be explained on the basis of a high concentration of dopant that could not be entirely incorporated in the crystalline network. It can also be stated that all powders are well crystallized and vanadium presence reduces the size of SnO_2 crystallites, aspect confirmed through the shape of the maxima (low intensity and large width). Further, the average crystallite size was estimated by using Scherrer equation, the resulting values being integrated in Table 1. Most of the calculated values for the doped samples are smaller than that of pure SnO_2. Moreover, the dopant type has an opposite effect on this structural parameter: the increase of lanthanum concentration is correlated with the growth of the average crystallite size, while the presence of vanadium in increasing proportion leads to lower average crystallite size. The result is not surprising taking into account the existing differences in ionic radius and valence for the two dopants.

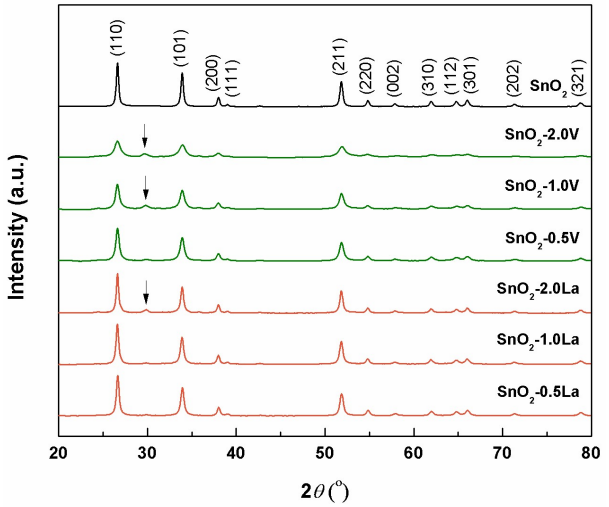

Fig. 2 - XRD patterns for SnO_2 calcined powders. The arrow indicates secondary phases / *Analizele de difracţie a razelor X pentru pulberile de SnO_2 calcinate. Săgeata indică faze secundare.*

The SEM images recorded on the calcined powders are shown in Figure 3. The powders consist of aggregates with different dimensions, typical of the precipitation method, which usually yields nanometric particles with high surface tension, particles that have the tendency to gather and agglomerate so that to reduce the free energy. The individual particles are quasi spherical or polyhedral, with sizes from several nanometers to tens of nanometers. Regarding the dopant influence on the morphological properties of SnO_2 powders, lanthanum causes the obtaining of larger and more rugged particles, while vanadium does not affect the particles shape and size.

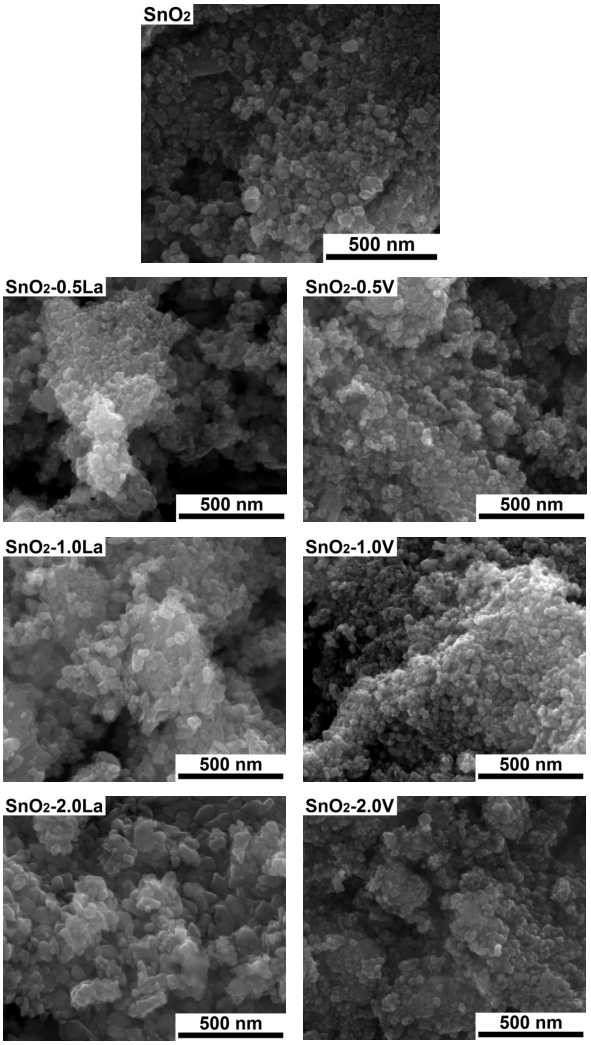

Fig. 3 - SEM images of SnO_2 calcined powders / *Imagini SEM ale pulberilor de SnO_2 calcinate.*

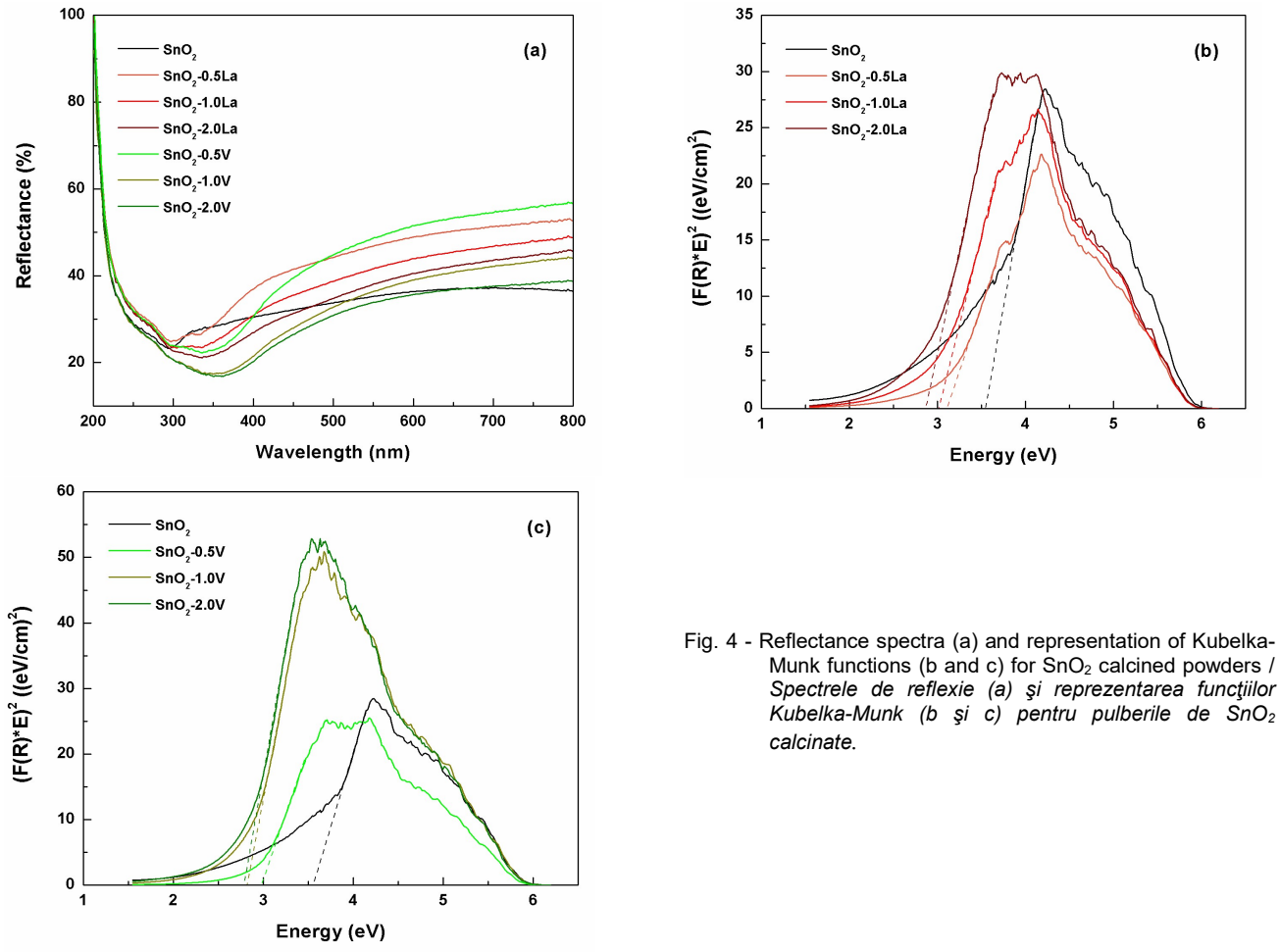

Fig. 4 - Reflectance spectra (a) and representation of Kubelka-Munk functions (b and c) for SnO_2 calcined powders / *Spectrele de reflexie (a) şi reprezentarea funcţiilor Kubelka-Munk (b şi c) pentru pulberile de SnO_2 calcinate.*

Table 1

Values of the average crystallite size and bandgap for SnO_2 calcined powders.
Valorile dimensiunii medii de cristalit şi ale benzii interzise pentru pulberile de SnO_2 calcinate.

Nr. *No.*	Dopant *Dopant*	Concentraţie (%grav.) *Concentration (wt.%)*	Dimensiune medie de cristalit (nm) *Average crystallite size* (nm)	Bandă interzisă (eV) *Bandgap (eV)*
1	-	-	53	3.55
2	La^{3+}	0.5	46	3.10
3		1.0	47	3.02
4		2.0	54	2.86
5	V^{5+}	0.5	36	2.98
6		1.0	32	2.82
7		2.0	21	2.78

Starting from the UV-Vis spectra of the calcined powders (Fig. 4 a) and employing Kubelka Munk graphical representations (Figs. 4 b and c), the values of the bandgap were extracted (linear extrapolation), being displayed in Table 1.

The doped powders present a left shift of the bandgap, namely a reduction of the bandgap as a consequence of dopant penetration into the crystalline network. Also, it is obvious that vanadium has a stronger influence, in other words a significant decrease of the bandgap even for a low dopant concentration.

The scientific literature already reported that when used as anode materials for Li-ion batteries, the doped samples show better electrochemical performance compared with pure SnO_2 particles due to a gradual decrease of the particle size with lanthanum content increasing from 1 to 10 % [26]. Another research group [27] stated that lanthanum doping prevents the growth of SnO_2 crystallites at concentrations lower than 5 at.%, it tends to dissolve in the bulk phase of SnO_2 to form a solid solution for concentrations below 10 at.%, whereas lanthanum disperses on the surface of SnO_2 as a monolayer when the concentration exceeds 10 at.%. Going to the second dopant, Sukunta *et al.* focused on the gas sensing results, which revealed that the response of SnO_2 nanoparticles in the presence of H_2S is significantly enhanced by vanadium doping at a very low concentration of 0.1 wt.% [28].

4.Conclusions

SnO_2 powders doped with La^{3+} or V^{5+} were successfully prepared by the precipitation method, followed by a calcination step at 400 °C. All powders consist of tetragonal SnO_2 with high crystallinity. The morphological investigation revealed particles with dimensions from several nanometers to tens of nanometers, as well as larger particles for lanthanum doping.

The presence of dopants led to both average crystallite size and bandgap reduction, the effects being more pronounced for the case of vanadium. The final materials exhibited bandgap values in the 2.78 - 3.55 eV range, which demonstrates that the dopant type and quantity influence the optical properties of SnO_2 based powders.

Such zero dimensional structures can be easily integrated in nanoscale devices for the gas sensors field, the functional properties being directly determined by the material properties, which can be tuned in the desired way via adequate processing parameters.

Acknowledgements

The SEM analyses on samples were possible due to EU-funding grant POSCCE-A2-O2.2.1-2013-1, Priority Direction 2, Project No. 638/12.c03.2014, Code SMIS-CSrNR 48652.

REFERENCES

1. G. Eranna, Metal oxide nanostructures as gas sensing devices, CRC Press, Boca Raton, 2012.
2. M Ippommatsu, H. Sasaki and H. Yanagida, Sensing mechanism of SnO_2 gas sensors, Journal of Materials Science, 1990, **25**, 259.
3. C. Busuioc, A. Evanghelidis, C. Florica and I. Enculescu, Influence of preparation steps on the properties of electrospun ZnO fibers, Digest Journal of Nanomaterials and Biostructures, 2014, **9**, 1569.
4. C. Busuioc, A. Evanghelidis, M. Enculescu and I. Enculescu, Optical and photocatalytic properties of electrospun ZnO fibers, Digest Journal of Nanomaterials and Biostructures, 2015, **10**, 957.
5. S. Das and V. Jayarman, SnO_2: A comprehensive review on structures and gas sensors, Progress in Materials Science, 2014, **66**, 112.
6. M. Batzill and U. Diebold, The surface and materials science of tin oxide, Progress in Surface Science, 2005, **79**, 47.
7. K. Rubenis, S. Populoh, P. Thiel, S. Yoon, U. Muller and J. Locs, Thermoelectric properties of dense Sb-doped SnO_2 ceramics, Journal of Alloys and Compounds, 2017, **692**, 515.
8. T.I. Gandhi, R.R. Babu, K. Ramamurthi and M. Arivanandhan, Effect of Mn doping on the electrical and optical properties of SnO_2 thin films deposited by chemical spray pyrolysis technique, Thin Solid Films, 2016, **598**, 195.
9. J.G. Kang, J.S. Park and H.J. Lee, Pt-doped SnO_2 thin film based micro gas sensors with high selectivity to toluene and HCHO, Sensors and Actuators B, 2017, **248**, 1011.
10. L.A. Ma, Z.H. Wei, X.Y. Ye, T. Lin and T.L. Guo, Structure and enhanced field emission properties of cone-shaped Zn-doped SnO_2 nanorod arrays on copper foil, Materials Letters, 2016, **174**, 32.
11. Z. Jiang, R. Zhao, B. Sun, G. Nie, H. Ji, J. Lei and C. Wang, Highly sensitive acetone sensor based on Eu-doped SnO_2 electrospun nanofibers, Ceramics International, 2016, **42**, 15881.
12. B. Babu, A.N. Kadam, R.V.S.S.N. Ravikumar and C. Byon, Enhanced visible light photocatalytic activity of Cu-doped SnO_2 quantum dots by solution combustion synthesis, Journal of Alloys and Compounds, 2017, **703**, 330.
13. X. Lian, Y. Li, X. Tong, Y. Zou, X. Liu, D. An and Q. Wang, Synthesis of Ce-doped SnO_2 nanoparticles and their acetone gas sensing properties, Applied Surface Science, 2017, **407**, 447.
14. P. Dou, Z. Cao, C. Wang, J. Zheng and X. Xu, Multilayer Zn-doped SnO_2 hollow nanospheres encapsulated in covalently interconnected three-dimensional graphene foams for high performance lithium-ion batteries, Chemical Engineering Journal, 2017, **320**, 405.
16. C. Busuioc and S.I. Jinga, Characterization of $LiZnVO_4$ ceramics prepared by two different methods, Journal of Optoelectronics and Advanced Materials, 2013, **15**, 1470.
17. G. Voicu, V.L. Ene, D.F. Sava, V.A. Surdu and C. Busuioc, Sol-gel derived vitroceramic materials for biomedical applications, Journal of Non-Crystalline Solids, 2016, **449**, 75.
18. V. Bilovol, C. Herme, S. Jacobo and A.F. Cabrera, Study of magnetic behaviour of Fe-doped SnO_2 powders prepared by chemical method, Materials Chemistry and Physics, 2012, **135**, 334.
19. S. Nilavazhagan, S. Muthukumaran and M. Ashokkumar, Structural, optical and morphological properties of La, Cu co-doped SnO_2 nanocrystals by co-precipitation method, Optical Materials, 2014, **37**, 425.
20. X. Zhong, B. Yang, X. Zhang, J. Jia and G. Yi, Effect of calcining temperature and time on the characteristics of Sb-doped SnO_2 nanoparticles synthesized by the sol-gel method, Particuology, 2012, **10**, 365.
21. P.V. Tuan, L.T. Hieu, L.Q. Nga, N.D. Dung, N.N. Ha and T.N. Khiem, Hydrothermal synthesis and characteristic photoluminescence of Er-doped SnO_2 nanoparticles, Physica B, 2016, **501**, 34.
22. Y.H. Cho, X. Liang. Y.C. Kang and J.H. Lee, Ultrasensitive detection of trimethylamine using Rh-doped SnO_2 hollow spheres prepared by ultrasonic spray pyrolysis, Sensors and Actuators B, 2015, **207**, 330.
23. M.S. Pereira, F.A.S. Lima, T.S. Ribeiro, M.R. da Silva, R.Q. Almeida, E.B. Barros and I.F. Vasconcelos, Application of Fe-doped SnO_2 nanoparticles in organic solar cells with enhanced stability, Optical Materials, 2017, **64**, 548.
24. A.P.S. Isabel, C.H. Kao, R.K. Mahanty, Y.C.S. Wu, C.Y. Li, C.Y. Lin and C.F. Lin, Sensing and structural properties of Ti-doped tin oxide (SnO_2) membrane for bio-sensor applications, Ceramics International, 2017, **43**, 10386.
25. S. Kitabayashi and N. Koga, Thermal decomposition of tin(II) oxyhydroxide and subsequent oxidation in air: Kinetic deconvolution of overlapping heterogeneous processes, The Journal of Physical Chemistry C, 2015, **119**, 16188.
26. C. Li, W. Wei, T. Xia, H. Wang, Y. Zhu and Y. Song, La-doped SnO_2: Synthesis and its electrochemical property, Journal of Rare Earths, 2010, **28**, 161.
27. C. Fu, J. Wang, M. Yang, X. Su, J. Xu and B. Jiang, Effect of La doping on microstructure of SnO_2 nanopowders prepared by co-precipitation method, Journal of Non-Crystalline Solids, 2011, **357**, 1172.
28. J. Sukunta, A. Wisitsoraat, A. Tuantranont, S. Phanichphant and C. Liewhiran, Highly-sensitive H_2S sensors based on flame-made V-substituted SnO_2 sensing films, Sensors and Actuators B, 2017, **242**, 1095.

****